AGU PUBLICATIONS

Geophysical Research Letters

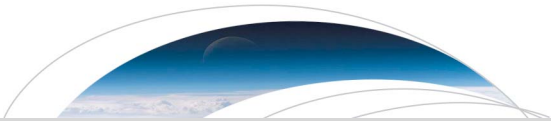

RESEARCH LETTER

10.1002/2017GL076817

Key Points:

- The distribution of spatial representativeness error is right-skewed for AERONET network
- Spatial representativeness error is 30% when constraining a model at a resolution of 2° × 2° with AERONET retrievals
- Spatial representativeness error is less for GAW or a subset of the AERONET sites outside of emission hot spots

Supporting Information:

- Supporting Information S1
- Data Set S1

Correspondence to:
R. Wang,
rongwang@fudan.edu.cn

Citation:
Wang, R., Andrews, E., Balkanski, Y., Boucher, O., Myhre, G., Samset, B. H., et al. (2018). Spatial representativeness error in the ground-level observation networks for black carbon radiation absorption. *Geophysical Research Letters*, *45*, 2106–2114. https://doi.org/10.1002/2017GL076817

Received 15 DEC 2017
Accepted 12 FEB 2018
Accepted article online 16 FEB 2018
Published online 28 FEB 2018

Spatial Representativeness Error in the Ground-Level Observation Networks for Black Carbon Radiation Absorption

Rong Wang[1,2,3], Elisabeth Andrews[4], Yves Balkanski[3], Olivier Boucher[5], Gunnar Myhre[6], Bjørn Hallvard Samset[6], Michael Schulz[7], Gregory L. Schuster[8], Myrto Valari[9], and Shu Tao[10]

[1]Department of Environmental Science and Engineering, Fudan University, Shanghai, China, [2]Department of Global Ecology, Carnegie Institution for Science, Stanford, CA, USA, [3]Laboratoire des Sciences du Climat et de l'Environnement, CEA CNRS UVSQ, Gif-sur-Yvette, France, [4]CIRES, University of Colorado, Boulder, CO, USA, [5]Institut Pierre-Simon Laplace, CNRS /Université Pierre et Marie Curie, Paris, France, [6]CICERO Center for International Climate and Environmental Research, Oslo, Norway, [7]Norwegian Meteorological Institute, Oslo, Norway, [8]NASA Langley Research Center, Hampton, VA, USA, [9]Laboratoire de Météorologie Dynamique, IPSL/CNRS, Ecole Polytechnique, Palaiseau, France, [10]Laboratory for Earth Surface Processes, College of Urban and Environmental Sciences, Peking University, Beijing, China

Abstract There is high uncertainty in the direct radiative forcing of black carbon (BC), an aerosol that strongly absorbs solar radiation. The observation-constrained estimate, which is several times larger than the bottom-up estimate, is influenced by the spatial representativeness error due to the mesoscale inhomogeneity of the aerosol fields and the relatively low resolution of global chemistry-transport models. Here we evaluated the spatial representativeness error for two widely used observational networks (AErosol RObotic NETwork and Global Atmosphere Watch) by downscaling the geospatial grid in a global model of BC aerosol absorption optical depth to 0.1° × 0.1°. Comparing the models at a spatial resolution of 2° × 2° with BC aerosol absorption at AErosol RObotic NETwork sites (which are commonly located near emission hot spots) tends to cause a global spatial representativeness error of 30%, as a positive bias for the current top-down estimate of global BC direct radiative forcing. By contrast, the global spatial representativeness error will be 7% for the Global Atmosphere Watch network, because the sites are located in such a way that there are almost an equal number of sites with positive or negative representativeness error.

Plain Language Summary When comparing the black carbon model at a resolution of 2° × 2° with local measurements, the global representativeness error is 30% for AErosol RObotic NETwork sites, compared to 7% for Global Atmosphere Watch sites. It demonstrates that, in absence of high-resolution models, the current top-down estimate of black carbon direct radiative forcing is overestimated by 30%.

1. Introduction

The role of black carbon (BC) in the climate system, in particular its direct radiative forcing, is highly debated (Boucher et al., 2016). The BC direct radiative forcing is often estimated from global aerosol transport models driven by emission inventories and subject to high uncertainties (Ghan et al., 2012; Kim et al., 2008; Myhre et al., 2013; Schulz et al., 2006; Wang, Jacob, et al., 2014). Therefore, high-quality measurements of BC aerosol absorption well distributed over the globe are needed to evaluate (Chen et al., 2017; Koch et al., 2009; Shindell et al., 2013) or constrain these models (Bond et al., 2013; Chung et al., 2005; Cohen & Wang, 2014; Sato et al., 2003).

Bottom-up approaches using chemistry-transport and climate models driven by emission inventories estimate the global BC direct radiative forcing at 0.1 to 0.5 W m^{-2} (Ghan et al., 2012; Kim et al., 2008; Myhre et al., 2013; Schulz et al., 2006; Wang, Jacob, et al., 2014), compared to 0.6 to 1.0 W m^{-2} in top-down approaches constrained by observations (Bond et al., 2013; Chung et al., 2005; Ramanathan & Carmichael, 2008; Sato et al., 2003). The main reason is that transport models generally underestimate the aerosol absorption optical depth (AAOD) of BC when comparing against a global measurement network—AErosol RObotic NETwork (AERONET) (Koch et al., 2009; Shindell et al., 2013), leading to ad-hoc adjustments in the bottom-up BC emissions (Bond et al., 2013; Cohen & Wang, 2014). However, the issue of the representativeness of the observations is generally overlooked in previous studies (Bond et al., 2013; Chung et al., 2005; Cohen &

Wang, 2014; Sato et al., 2003). Spatial representativeness error (RE) is induced by using measurements at one site to represent an average over one region, typically a coarse model grid box, and this error arises because of the mesoscale inhomogeneity of the aerosol fields (Anderson et al., 2003). For example, it is a common practice to compare the modeled BC AAOD over a grid box of approximately 2° × 2° with measurements at a local site (Bond et al., 2013; Chung et al., 2005; Cohen & Wang, 2014; Sato et al., 2003).

While the spatial RE has been widely considered in the field of carbon dioxide data assimilation (Gerbig et al., 2003; Lin et al., 2006), it has also occasionally been considered for atmospheric aerosols (Schutgens, Gryspeerdt, et al., 2016; Schutgens et al., 2017; Wang et al., 2016). Recently, Schutgens, Gryspeerdt, et al. (2016) explored the spatial REs for simulated aerosol optical depth (AOD) and surface BC concentrations by comparing a small 10 km × 10 km model grid to the average of a large 210 km × 210 km model grid surrounding it. However, that study was limited to six regions, making it hard to evaluate the RE associated with a global observational network like AERONET (Schutgens, Gryspeerdt, et al., 2016). Wang et al. (2016) developed a global field of BC AAOD for year 2007 at a resolution of 0.1° × 0.1°, which reduced the discrepancy between the modeled and observed BC AAOD. However, that study did not systematically assess the RE in AERONET and left the impact on the current top-down estimate of BC direct radiative forcing constrained by AERONET unknown (Wang et al., 2016).

Here we used a recently published data set for annual mean (for year 2007) BC AAOD at a high resolution of 0.1° × 0.1° (Wang et al., 2016) to assess the spatial RE when using the retrievals of AAOD at AERONET sites to constrain models at a coarse resolution from 1° × 1° to 3° × 3°. For a comparison, we assessed the error associated with sites in the Global Atmosphere Watch (GAW) network.

2. Methods

2.1. A Global 0.1° × 0.1° Field of BC AAOD for Year 2007

Global distribution of BC AAOD at 900 nm for the year 2007 was downscaled to a horizontal resolution of 0.1° × 0.1°. Our downscaling technique involves a global chemistry transport and climate model LMDZ-OR-INCA with a nest region in Asia (Wang et al., 2016), a global emission data set constructed at a resolution of 0.1° × 0.1° (Wang, Tao, et al., 2014) and a regional chemical transport model CHIMERE run at a resolution of 0.1° × 0.1° (Menut et al., 2013). The two-step methodology used in constructing the 0.1° × 0.1° global field of BC AAOD was detailed in Wang et al. (2016) and is described briefly below.

In a first step, we ran the LMDZ-OR-INCA model (Schulz et al., 2006; Balkanski et al., 2010) at two different horizontal resolutions, including one zoomed over Asia with a horizontal resolution of 0.51° latitude by 0.66° longitude for a region (70°E–130°E, 7°N–45°N) and another one with a fixed resolution of 1.27° latitude by 2.50° longitude globally. A state-of-the-art global emission inventory of BC at a native resolution of 0.1° × 0.1° compiling subnational emission data (Wang, Jacob, et al., 2014) was used to drive the two simulations. In addition, the aerosol optics scheme in LMDZ-OR-INCA was improved by treating BC as internally mixed with primary organic matter and sulfate with the equivalent refractive index calculated by the Maxwell Garnett mixing rule (Chýlek et al., 1988). This generated a global map of BC AAOD at a resolution of 0.51° × 0.66° over the zoomed Asian region from the zoomed model and at a resolution of 1.27° × 2.50° elsewhere from the regular model.

In a second step, we downscaled the global map of BC AAOD derived from the first step to 0.1° × 0.1° grids using an exponential interpolation method based on the 0.1° × 0.1° map of BC emission density. We assumed that the distribution of BC AAOD is proportional to the emission density with an exponential coefficient (α). With α, we wrote the downscaled BC AAOD for a 0.1° × 0.1° subgrid as

$$\mathrm{AAOD}_i = \mathrm{AAOD}_x \cdot \frac{(E_i)^{\alpha}}{\sum_i \left[A_{i,x} \cdot (E_i)^{\alpha}\right]}, \tag{1}$$

where i denotes the 0.1° × 0.1° subgrid, x denotes the coarse model grid (at a resolution of 0.51° × 0.66° in Asia and 1.27° × 2.50° elsewhere), E_i is the BC emission density in the 0.1° × 0.1° subgrid, and $A_{i,x}$ is the fractional area of the subgrid i in the model grid x. The closer the value of α is to zero, the smoother the BC AAOD is in space relative to the source distribution. Because equation (1) only considers the impact of local emissions on the spatial distribution, it will cause a bias in the modeled BC AAOD at sites where local sources contribute

less to BC AAOD than sources outside of the model grid box. Then, a regional CHIREME model (Menut et al., 2013) was run over the North China Plain at a resolution of 0.1° × 0.1° with the BC emission inventory of Wang, Tao, et al. (2014) to assess the error in the downscaling. The optimal parameter (α) was obtained by minimizing deviations between the interpolated BC column burden (as a proxy for BC AAOD) and that modeled by CHIMERE over the North China Plain. The optimized (α) was applied for downscaling the modeled BC AAOD from all model grids (0.51° × 0.66° in Asia and 1.27° × 2.50° elsewhere) to 0.1° × 0.1° grids over continents. Due to the heavy computational demand of running a 0.1° × 0.1° global simulation, calibration of the parameter (α) was only done over the North China Plain in our study. To reduce this bias, until global simulations are made available at 0.1° × 0.1° resolution, such calibration of (α) could be done over different regions in future studies. Figure S1 in the supporting information shows the resulting 0.1° × 0.1° field of BC AAOD.

Wang et al. (2016) showed that, relative to the same aerosol model (Schulz et al., 2006) run at a coarse resolution of 1.2° × 2.5° driven by an emission inventory of BC at a native resolution of 0.5° × 0.5° (Lamarque et al., 2010), the new 0.1° × 0.1° data of BC AAOD can reduce the normalized mean bias in BC AAOD relative to AERONET from −51% to −5% in Asia and less significantly from −57% to −36% in other regions. Figure S2 shows that high values near a hot spot site (Beijing as an example) are well captured by CHIMERE. Figure S3 shows that the frequency distribution of BC AAOD at all AERONET sites in our 0.1° × 0.1° data set agrees better with the retrievals than the frequency distribution modeled at a coarse resolution of 1.2° × 2.5°.

2.2. Representativeness Error for AERONET and GAW Sites

Measurement networks that provide aerosol absorption include GAW (WMO, 2016) measurements of the aerosol absorption coefficient and the AERONET (Dubovik & King, 2000; Holben et al., 1998) retrievals of AAOD. The GAW and AERONET networks measure absorbing aerosols at 92 (with 9 urban sites) and 591 (with 207 urban sites) sites, respectively (Figure S4). To identify the GAW sites making absorbing aerosol measurements, we searched for "aerosol optical properties/aerosol absorption" and "aerosol composition/inorganic carbonaceous/elemental carbon" on the GAWSIS webpage (https://gawsis.meteoswiss.ch/GAWSIS//index.html) and searched for "aerosol absorption coefficient" and "equivalent BC" on the EBAS webpage (ebas.nilu.no). Note that this number of AERONET sites is for year 2013 compiled in our previous study (Wang et al., 2016), where missing refractive indices in version 2.0 product were recovered from version 1.5 product. By 2017 AERONET had expanded to 1383 sites on the website (some of those sites are not operational), for which the information segregating urban and nonurban sites is unavailable.

Kinne et al. (2013) assigned a range score to indicate the ability of local sites in the AERONET network to represent properties beyond the local grid and a quality score to indicate the accuracy of the data. The Kinne et al. grading system resulted in 258 valid sites, less than our list for three reasons: It only includes sites with Sun-data coverage for >5 months of the year, it only covers data up to 2008, and it ignores sites with the quality score of zero (e.g., high-altitude mountain sites). Here we also assess the RE associated with the 258 sites used by Kinne et al. (2013) and computed the RE as a function of the range score.

In the absence of high-resolution observations at the global scale (e.g., from satellites), we used our downscaled BC AAOD at the 0.1° × 0.1° resolution as synthetic observations. We approximated the annual mean BC AAOD at a local site by the value of the 0.1° × 0.1° grid box it belongs to, namely, $C_{\text{high-res}}$. We then estimated the annual mean BC AAOD over a low-resolution grid box of $g° \times g°$, namely, $C_{\text{low-res}}$, as the average over $n = (10\ g)^2$ 0.1° × 0.1° grid boxes with the monitoring site closest to the center. Figure S5 shows a schematic of how $C_{\text{high-res}}$ and $C_{\text{low-res}}$ are calculated. We defined the RE as

$$RE = \frac{C_{high-res} - C_{low-res}}{C_{low-res}}, \tag{2}$$

An RE of zero indicates that the site is perfectly representative of the coarse grid box. The magnitude of RE indicates the departure from representativeness, and the sign of RE indicates whether the site has lower (negative) or higher (positive) loading than the surrounding grid boxes.

The lists of three sets of AERONET sites and the GAW sites are provided in the Supporting Spreadsheet along with the site information and the calculated RE values.

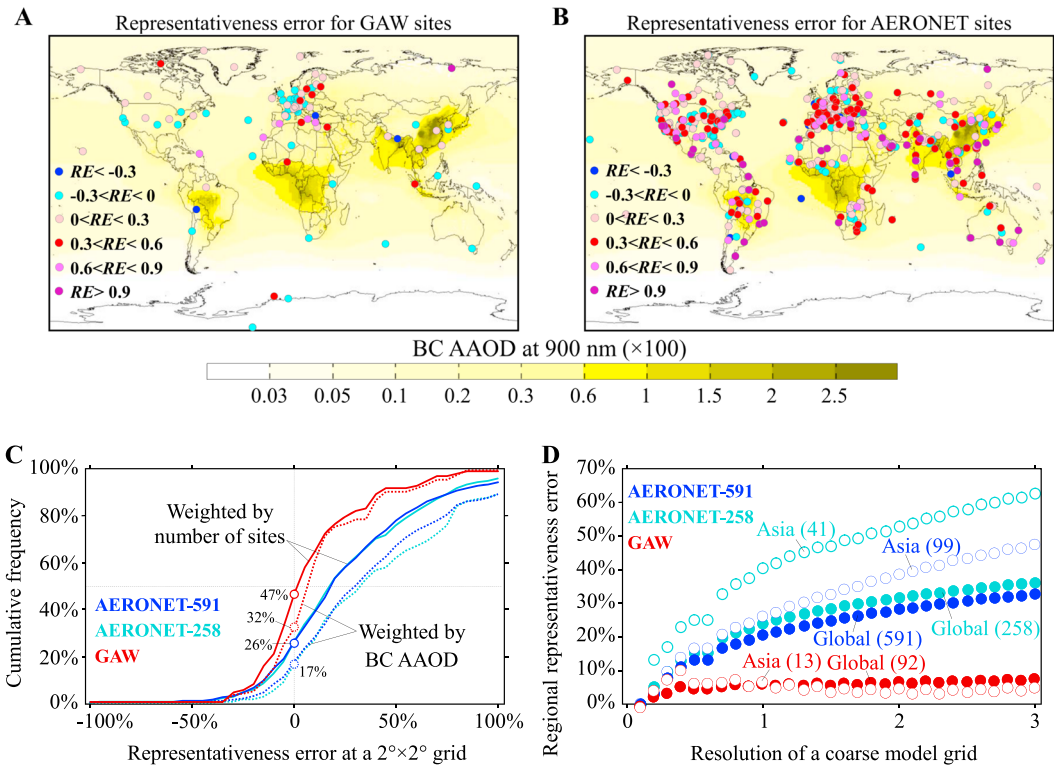

Figure 1. Evaluation of the representativeness error for the AErosol RObotic NETwork (AERONET) and Global Atmosphere Watch (GAW) networks. (A and B) Representativeness error computed when using modeled black carbon (BC) aerosol absorption optical depth (AAOD) from a 0.1° × 0.1° grid as representative of a 2° × 2° coarse model-grid for each (a) GAW and (b) AERONET site. The 0.1° × 0.1° BC AAOD field is shown by the color bar. (c) Cumulative frequency distributions of the representativeness error (RE) using BC AAOD over a 2° × 2° grid box relative to a 0.1° × 0.1° resolution positioned at GAW (red) and AERONET (blue or cyan) sites. The distributions are weighted by the number of sites (solid lines) or modeled BC AAOD (dash lines). A vertical dotted line at 0 and a horizontal dotted line at 50% are plotted to show the asymmetry. The labels next to circles denote the percentages of negative RE. (d) Dependence of the regional representativeness error on the grid resolution relative to 0.1° × 0.1° grid boxes for all sites (solid circles) and Asian sites (open circles) of the GAW (red) and AERONET (blue or cyan) networks. The number of sites is listed in parentheses. (C and D) For AERONET, we compare the result by using 591 sites (blue) covering data up to 2013 by Wang et al. (2016) or 258 sites (cyan) covering data up to 2008 by Kinne et al. (2013).

3. Results

3.1. Quantification of the Representativeness Error

Based on the 0.1° × 0.1° field of BC AAOD (annual mean) for year 2007, Figures 1a and 1b plot the RE for a 2° × 2° resolution (g = 2) at each GAW and AERONET site. In Figures 1a and 1b, the modeled BC AAOD is shown as a background. There are two implications for the RE. First, the simulated BC AAOD will be underestimated in a 2° × 2° model for each site with positive *RE* and overestimated for each site with negative RE. Second, when constraining the regional BC direct radiative forcing as done by Bond et al. (2013), the modeled BC AAODs are averaged over 2° × 2° to be compared over measuring sites in each region. Thus, if an observational network dominated by sites with positive (resp. negative) RE is used to constrain the model, the representativeness issue will lead to an overestimation (resp. underestimation) in the constrained BC AAOD averaged over the region. To constrain the regional BC direct radiative forcing, as done by Bond et al. (2013), using a network more evenly distributed between sites with positive and negative REs can lead to a lower bias than that using a network dominated by sites with positive (resp. negative) RE.

Figures 1a and 1b show that AERONET locates a significant number of sites in emission hot spots that are subject to high RE. In contrast, the GAW network contains almost the same number of sites with a positive or negative RE. Figure 1c shows the cumulative frequency distribution of RE for 92 GAW and 591 AERONET

sites for a 2° × 2° resolution (g = 2) (see Figure S6 for the probability density function distributions). It shows that RE, weighted by the number of sites, has a right-skewed distribution in AERONET with 74% sites subject to a positive RE, in contrast to 53% sites with a positive RE in GAW. It means that using the BC absorption data measured at GAW sites to constrain the global BC direct radiative forcing should be less biased than AERONET. Weighting by the modeled BC AAOD (dotted lines in Figure 1c) shifts the two distribution curves to the right, increasing the percentage of positive RE to 83% of the AERONET sites and 68% of the GAW sites, respectively. This indicates that sites with high BC AAOD are more likely to have a higher positive RE relative to sites with low BC AAOD.

Figure S7 shows that the distribution of RE for AERONET changes slightly if we use the 1,383 sites in 2017 for the calculation, with the same fraction (74%) of sites subject to a positive RE. Figure S8 shows an example of how the RE increases from −11% for a nonurban site to 80% for an urban site (Beijing) over an emission hot spot region. Keep in mind that not all AERONET sites are able to provide valid measurements of BC AAOD due to lack of measured single scattering albedo under low AOD or other operational reasons (Dubovik & King, 2000). Kinne et al. (2013) had selected 258 sites with Sun-data coverage for >5 months of the year and nonzero quality score. We calculated the RE based on these 258 sites, of which, again, 74% are subject to a positive RE (Figure 1c).

To quantify the RE at the regional scale, we used $C_{\text{high-res}}$ and $C_{\text{low-res}}$ derived above to compute their averages, namely, $\overline{C_{\text{high-res}}}$ and $\overline{C_{\text{low-res}}}$, in five regions (the Americas, Europe, Africa, and Asia; see Figure S4 for a map). We then computed the regional RE as RRE = $(\overline{C_{\text{high-res}}} - \overline{C_{\text{low-res}}})/\overline{C_{\text{low-res}}}$, as a function of the resolution of a coarse model grid ($g° \times g°$), as shown in Figure 1d for the globe and for Asia. Figure S9 shows the RRE with the variance of RE of sites in each region. For the full data set and for Asian sites, RRE increases dramatically with model resolution for the AERONET network, while it remains smaller for the GAW network. When constraining the model at a resolution of 2° × 2°, the average RRE is 28% for all AERONET sites, compared to 7% for all GAW sites. Using the 258 AERONET sites with higher frequencies of BC AAOD retrievals, the RRE is estimated at 53% in Asia and 32% globally, which can be compared with 39% and 28% respectively for the 591 sites (Figure 1d). This confirms higher spatial RE for the AERONET network than for GAW. Regionally, RRE is largest in Asia for AERONET with a large number of sites located in emission hot spots (Figure S9).

Although the estimated RRE for GAW is lower than that for AERONET, it does not mean that GAW is better suited than AERONET to constrain global models. First, while we interpolated BC AAOD from 50 to 10 km in Asia based on emissions, the impact of orography is not accounted for. Mountain sites are less representative than other sites. On the one hand, the atmospheric column at mountain sites is lower than that in lowlands surrounding the mountain (Whiteman, 2000); on the other hand, mountains may act as a barrier to the transport of aerosol (Silcox et al., 2012). For example, we calculated RE to be −0.04 at a GAW site located in a depression surrounded by mountains with few BC sources nearby (Assekrem, 23.26°N, 5.63°E), which may be underestimated due to the orography. After removing sites with an elevation over 500 m, global RRE increases from 7% (92 sites) to 11% (56 sites) for the GAW network, and from 28% (1383 sites) to 30% (1065 sites) for the AERONET network. Second, there are fewer sites in the GAW network than AERONET. While the current top-down approach (Bond et al., 2013) compares the modeled BC AAOD as an average over sites in each region with measurements, the issue of how these sites represent the whole region is not assessed and is beyond the scope of this current paper. Applying an approach to use information at all sites, like Chevallier et al. (2005) and Huneeus et al. (2013), can help us further understand the importance of high-resolution modeling in reducing uncertainty in the top-down radiative forcing of BC in future studies.

Finally, while we are assessing the spatial RE, we should note that there could also be a temporal RE if the modeled annual mean BC AAOD was compared with the measurements for just a few days (Chin et al., 2002). Schutgens, Partridge, & Stier (2016) showed that temporal sampling errors in yearly and monthly mean AODs for AERONET amount to 20–90%, with smaller sampling errors in the daily averages. Schutgens et al. (2017) suggest that temporal sampling errors can be even larger than spatial sampling errors at some sites, which should be accounted for when using measurements to constrain the models.

3.2. Factors Leading to the Representativeness Error

The spatial RE arises from the inhomogeneous distribution of BC within a coarse model grid box and increases model bias with respect to local measurements. Our downscaling of a global simulation of BC

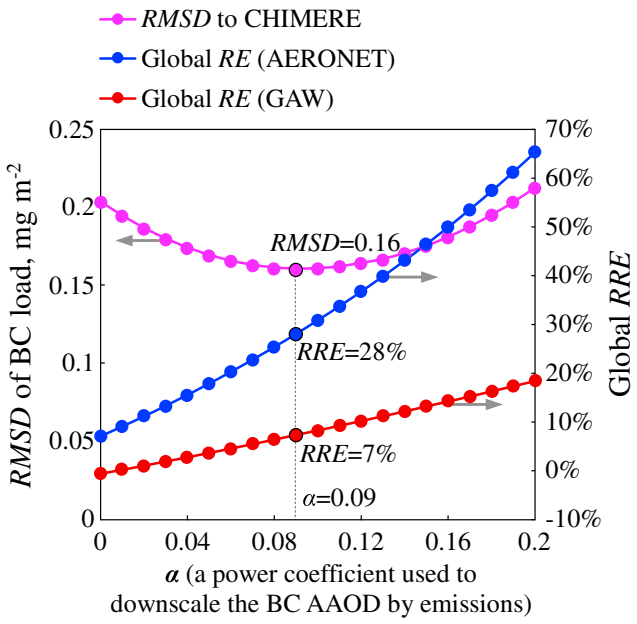

Figure 2. Dependence of the root mean square deviation (RMSD) between the downscaled black carbon (BC) load (as a proxy for BC aerosol absorption optical depth) and the CHIMERE data (purple circles) on α is shown on the left axis. Dependence of the global regional representativeness error (RRE) for the AErosol RObotic NETwork (591 sites, blue circles) and Global Atmosphere Watch (92 sites, red circles) networks on α is shown in the right axis.

AAOD shows that this RE is notable when compared to models at a resolution of 1 to 3° in latitude and longitude at the AERONET sites. In our study, the distribution of BC AAOD within a coarse model grid box is mainly induced by the distribution of emissions. Since a transported, atmospherically mixed property like BC AAOD should be smoother than its source distribution, we introduced a method to downscale BC AAOD from coarse model grids to 0.1° × 0.1° with a fixed coefficient (α) (see equation (1) in section 2). A regional model, CHIMERE (Menut et al., 2013), was run at a resolution of 0.1° × 0.1° to assess the error in the downscaling. Figure 2 shows that the root-mean-square deviation between the downscaled BC load (as a proxy for BC AAOD) and the CHIMERE data increases as α increases initially and then declines. Meanwhile, the global RRE for both AERONET (591 sites) and GAW (92 sites) networks increases as the parameter (α) increases, as a result of our downscaling method based upon emissions. Since the CHIMERE data provide a constraint on the value of α, we obtained an optimal α = 0.09 with the best agreement between the downscaled method and the CHIMERE data, leading to a global REE of 28% and 7% for the AERONET and GAW networks, respectively. Note that we used the modeled BC AAOD at a resolution of 0.1° × 0.1° to approximate local measurements. It is likely that there remains subgrid scale variability in BC AAOD even at the 0.1° × 0.1° resolution, which could still lead to greater or lower spatial RE than estimated here.

The fact that many AERONET sites cannot be seen as representative of their surrounding area has been noticed previously. For example, Kinne et al. (2013) assigned a range score for each site, where a score of 0, 1, 2, and 3 indicated that the site was representative for a domain of 1° × 1°, 3° × 3°, 5° × 5°, and 9° × 9° grid box, respectively. Figure 3a compares the RE calculated for sites with different range scores. It shows that the likelihood of a site having a large RE is significantly higher for sites with a range score of 0 or 1 than for sites with a range score of 2 or 3. For example, the 5% and 95% percentiles of *RE* are −26% and 100% for sites with a range score of 1, indicating that 10% of these sites are subject to an RE of <−26% or >100%. By contrast, the 5% and 95% percentiles of RE are −0.5% and 40% for sites with a range score of 3. Figure 3b shows that the distribution of RE for urban sites in AERONET is severely right-skewed, with 92% of urban sites subject to a positive RE, in contrast to 64% of nonurban sites. This is consistent with Kinne et al. (2013) that urban sites are associated with a lower range score and thus representative of a smaller region in space.

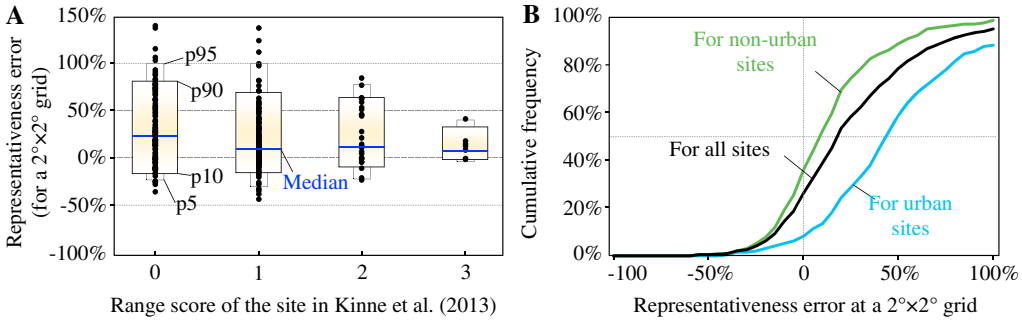

Figure 3. (a) Representativeness error at a 2° × 2° grid box for the AErosol RObotic NETwork (AERONET) sites with different range scores given by Kinne et al. (2013). The bars show the 5%, 10%, 90%, and 95% percentiles, and the horizontal lines show the median. (b) Cumulative frequency distributions of the representativeness error using black carbon aerosol absorption optical depth over a 2° × 2° grid box relative to a 0.1° × 0.1° resolution positioned at AERONET measurement sites. The black line uses all sites, the blue line uses urban sites, and the green line uses nonurban sites.

While Figures 2 and 3 illustrate the effect of emission sources on RE, there are other factors that can cause the inhomogeneous distribution of BC in a model grid, such as meteorology and orography. For example, Schutgens et al. (2017) suggested that large REs in the Alps, the Apennines, and the Carpathian mountains are related to orography. While orography is an important reason, we propose that the fact that local emissions in mountainous regions are often lower than the surrounding regions can also contribute to negative RE at these mountain sites. Kinne et al. (2013) excluded all high-altitude mountain sites, because they cannot represent the $1° \times 1°$ grid. In our study, among the 591 AERONET sites, the average RE is $-1.4 \pm 31.4\%$ for the 7 mountainous sites, which is lower than $28.5 \pm 43.2\%$ for other sites.

Our study shows that spatial variability in emission sources is capable of generating significant mesoscale variation in aerosol that in turn leads to sizable REs. Among various inputs needed to estimate the spatial distribution of anthropogenic emissions, population and road network data are essential. Mainstream bottom-up inventories (Bond et al., 2013; Lamarque et al., 2010) use the spatial distribution of population as a proxy for emissions of various species from specific sectors, because there is a high-quality data set for population at a high resolution (~1 km) (Oak Ridge National Laboratory., 2017). More mesoscale measurements (Anderson et al., 2003) to quantify the relationship between aerosol absorption and population density would be helpful for devising a framework to assess the spatial representativeness of measurement sites.

4. Conclusion and Implications

In this study, we assessed the RE for absorbing aerosol associated with two observational networks (AERONET and GAW) that are used to constrain global models at a coarse resolution. By considering the impact of spatial variability in BC emissions on AAOD representativeness, our results show that the distribution of RE is right-skewed for the AERONET network. When comparing the model at a resolution of $2° \times 2°$ with measurements, the RE in the BC AAOD averaged over global sites is 30% for the AERONET network, compared to 7% for the GAW network. It indicates that, when constraining the models at a resolution of around $2° \times 2°$ with measurements at all AERONET sites, the current top-down estimate of BC direct radiative forcing is overestimated by 30% (Bond et al., 2013; Chung et al., 2005; Sato et al., 2003), which explains a part of the difference between top-down and bottom-up BC direct radiative forcing estimates. In contrast, the GAW network or a subset of the AERONET sites is less influenced by RE and provides valuable constraints on the modeled global BC radiative forcing. Such a representative error analysis could be used to guide the design of networks with sites distributed both in polluted and remote regions (Silva & Quiroz, 2003; Trujillo-Ventura & Ellis, 1991; Wu et al., 2010).

In addition to AAOD, AERONET measures AOD, which is dominated by sulfate, nitrate, primary organic carbon, BC, and dust. The AOD data are also widely used to constrain the models (e.g., Kinne et al., 2013; Shindell et al., 2013). Although AOD is contributed by more natural sources (e.g., natural dust and sea salt) than BC, some of these species or their precursors are co-emitted with BC in the urban regions and their lifetime is close to BC. Thus, we expect that measurements of AOD in AERONET may also be associated with an RE at urban sites when constraining low-resolution models. To assess the RE in the measured AOD, further efforts are needed to construct high-resolution fields of all aerosol species by developing consistent emission inventories (e.g., Huang et al., 2015; Meng et al., 2017) and high-resolution models.

There are some limitations in our work. First, while we assessed the spatial variability of BC caused by emissions, other factors causing RE are not accounted for. For example, when we interpolated the BC AAOD field from a scale of 50 to 10 km in Asia based on emissions, the effects of local chemical processing, physical removal (precipitation) (Anderson et al., 2003), and orography (Schutgens et al., 2017) at a scale below 50 km are not considered. Second, AAOD measurements are always made during a small part of the day. Comparing them to daily or monthly model averages will introduce additional temporal RE (Schutgens, Partridge, & Stier, 2016), which is unquantified in our study. Third, while we estimated the spatial RE using a previous method that constrains the model by region, an inversion approach using information at all sites is needed to quantify the influence of the number of sites in the network (Chevallier et al., 2005; Huneeus et al., 2013). At last, measurements of BC AAOD cannot constrain the vertical profiles of BC, which are crucial for the estimation of direct radiative forcing (Samset et al., 2013). Further studies should overcome these limitations to deliver a top-down estimation of BC direct radiative forcing. Nevertheless,

our study highlights the importance of developing high-resolution transport models in the inversion of aerosols and the design of the observational networks for such a purpose.

Abbreviations

BC	black carbon
AERONET	AErosol RObotic NETwork
GAW	Global Atmosphere Watch
AAOD	aerosol absorption optical depth
AOD	aerosol optical depth
RE	representativeness error
RRE	regional representativeness error
$C_{\text{high-res}}$	annual mean BC AAOD over a high-resolution grid box of 0.1° × 0.1°
$C_{\text{low-res}}$	annual mean BC AAOD over a low-resolution grid box of g° × g°

Acknowledgments
In this study, R.W. was funded by the Chinese "Thousand Youth Talents" Program grant, the Fund for Innovative Climate and Energy Research, and the Marie Curie International Incoming Fellowship funded by the European Commission (project 628735); E.A. was supported by NOAA Climate Program Office's Atmospheric Chemistry, Carbon Cycle and Climate (AC4) program; G.M. was supported through the Norwegian Research Council project SUPER (grant 250573/F20); B.H.S. was supported by the Research Council of Norway (grant 240372). The simulations were performed using supercomputing resources from the GENCI (Grand Equipement National de Calcul Intensif) under grant 2016-t2014012201. The lists of AERONET and GAW sites used in this study were provided in the Supporting Spreadsheet, while information for AERONET sites were downloaded from http://aeronet.gsfc.nasa.gov/ and information for GAW sites were downloaded from https://gawsis.meteoswiss.ch/GAWSIS//index.html and ebas.nilu.no.

References

Anderson, T. L., Charlson, R. J., Winker, D. M., Ogren, J. A., & Holmen, K. (2003). Mesoscale variations of tropospheric aerosols. *Journal of the Atmospheric Sciences*, *60*(1), 119–136. https://doi.org/10.1175/1520-0469(2003)060%3C0119:MVOTA%3E2.0.CO;2

Balkanski, Y., Myhre, G., Gauss, M., Radel, G., Highwood, E. J., & Shine, K. P. (2010). Aerosol emitted by transport: direct radiative effect from road, ships and aviation. *Atmospheric Chemistry and Physics*, *10*, 4477–4489. https://doi.org/10.5194/acp-10-4477-2010

Bond, T. C., Doherty, S. J., Fahey, D. W., Forster, P. M., Berntsen, T., DeAngelo, B. J., et al. (2013). Bounding the role of black carbon in the climate system: A scientific assessment. *Journal of Geophysical Research: Atmospheres*, *118*, 5380–5552. https://doi.org/10.1002/jgrd.50171

Boucher, O., Balkanski, Y., Hodnebrog, Ø., Myhre, C. L., Myhre, G., Quaas, J., et al. (2016). Jury is still out on the radiative forcing by black carbon. *Proceedings of the National Academy of Sciences of the United States of America*, *113*(35), E5092–E5093. https://doi.org/10.1073/pnas.1607005113

Chen, B., Zhu, Z., Wang, X., Andersson, A., Chen, J., Zhang, Q., & Gustafsson, Ö. (2017). Reconciling modeling with observations of radiative absorption of black carbon aerosols. *Journal of Geophysical Research: Atmospheres*, *122*, 5932–5942. https://doi.org/10.1002/2017JD026548

Chevallier, F., Engelen, R. J., & Peylin, P. (2005). The contribution of AIRS data to the estimation of CO_2 sources and sinks. *Geophysical Research Letters*, *32*, L23801. https://doi.org/10.1029/2005GL024229

Chin, M., Ginoux, P., Kinne, S., Torres, O., Holben, B. N., Duncan, B. N., et al. (2002). Tropospheric aerosol optical thickness from the GOCART model and comparisons with satellite and Sun photometer measurements. *Journal of Atmospheric Science*, *59*(3), 461–483.

Chung, C. E., Ramanathan, V., Kim, D., & Podgorny, I. A. (2005). Global anthropogenic aerosol direct forcing derived from satellite and ground-based observations. *Journal of Geophysical Research*, *110*, D24207. https://doi.org/10.1029/2005JD006356

Chýlek, P., Srivastava, V., Pinnick, R. G., & Wang, R. T. (1988). Scattering of electromagnetic waves by composite spherical particles: Experiment and effective medium approximations. *Applied Optics*, *27*(12), 2396–2404. https://doi.org/10.1364/AO.27.002396

Cohen, J. B., & Wang, C. (2014). Estimating global black carbon emissions using a top-down Kalman filter approach. *Journal of Geophysical Research: Atmospheres*, *119*, 307–323. https://doi.org/10.1002/2013JD019912

Dubovik, O., & King, M. D. (2000). A flexible inversion algorithm for retrieval of aerosol optical properties from Sun and sky radiance measurements. *Journal of Geophysical Research*, *105*(D16), 20,673–20,696. https://doi.org/10.1029/2000JD900282

Gerbig, C., Lin, J. C., Wofsy, S. C., Daube, B. C., Andrews, A. E., Stephens, B. B., et al. (2003). Toward constraining regional-scale fluxes of CO2 with atmospheric observations over a continent: 1. Observed spatial variability from airborne platforms. *Journal of Geophysical Research*, *108*, 4756. https://doi.org/10.1029/2002JD003018

Ghan, S. J., Liu, X., Easter, R. C., Zaveri, R., Rasch, P. J., & Yoon, J. H. (2012). Toward a minimal representation of aerosols in climate models: Comparative decomposition of aerosol direct, semidirect, and indirect radiative forcing. *Journal of Climate*, *25*(19), 6461–6476. https://doi.org/10.1175/JCLI-D-11-00650.1

Holben, B. N., Eck, T. F., Slutsker, I., Tanré, D., Buis, J. P., Setzer, A., et al. (1998). AERONET—A federated instrument network and data archive for aerosol characterization. *Remote Sensing of Environment*, *66*(1), 1–16. https://doi.org/10.1016/S0034-4257(98)00031-5

Huang, Y., Shen, H., Chen, Y., Zhong, Q., Chen, H., Wang, R., et al. (2015). Global organic carbon emissions from primary sources from 1960 to 2009. *Atmospheric Environment*, *122*, 505–512. https://doi.org/10.1016/j.atmosenv.2015.10.017

Huneeus, N., Boucher, O., & Chevallier, F. (2013). Atmospheric inversion of SO_2 and primary aerosol emissions for the year 2010. *Atmospheric Chemistry and Physics*, *13*(13), 6555–6573. https://doi.org/10.5194/acp-13-6555-2013

Kim, D., Wang, C., Ekman, A. M. L., Barth, M. C., & Rasch, P. J. (2008). Distribution and direct radiative forcing of carbonaceous and sulfate aerosols in an interactive size-resolving aerosol-climate model. *Journal of Geophysical Research*, *113*, D16309. https://doi.org/10.1029/2007JD009756

Kinne, S., O'Donnel, D., Stier, P., Kloster, S., Zhang, K., Schmidt, H., et al. (2013). MAC-v1: A new global aerosol climatology for climate studies. *Journal of Advances in Modeling Earth Systems*, *5*, 704–740. https://doi.org/10.1002/jame.20035

Koch, D., Schulz, M., Kinne, S., McNaughton, C., Spackman, J. R., Balkanski, Y., et al. (2009). Evaluation of black carbon estimations in global aerosol models. *Atmospheric Chemistry and Physics*, *9*(22), 9001–9026. https://doi.org/10.5194/acp-9-9001-2009

Lamarque, J. F., Bond, T. C., Eyring, V., Granier, C., Heil, A., Klimont, Z., et al. (2010). Historical (1850–2000) gridded anthropogenic and biomass burning emissions of reactive gases and aerosols: Methodology and application. *Atmospheric Chemistry and Physics*, *10*(15), 7017–7039. https://doi.org/10.5194/acp-10-7017-2010

Lin, J. C., Gerbig, C., Wofsy, S. C., Daube, B. C., Matross, D. M., Chow, V. Y., et al. (2006). What have we learned from intensive atmospheric sampling field programmes of CO_2? *Tellus B*, *58*(5), 331–343. https://doi.org/10.1111/j.1600-0889.2006.00202.x

Meng, W. J., Zhong, Q. R., Yun, X., Zhu, X., Huang, T. B., Shen, H. Z., et al. (2017). Improvement of a global high-resolution ammonia emission inventory for combustion and industrial sources with new data from the residential and transportation sectors. *Environmental Science & Technology*, *51*(5), 2821–2829. https://doi.org/10.1021/acs.est.6b03694

Menut, L., Bessagnet, B., Khvorostyanov, D., Beekmann, M., Blond, N., Colette, A., et al. (2013). CHIMERE 2013: A model for regional atmospheric composition modeling. *Geoscientific Model Development*, *6*(4), 981–1028. https://doi.org/10.5194/gmd-6-981-2013

Myhre, G., Samset, B. H., Schulz, M., Balkanski, Y., Bauer, S., Berntsen, T. K., et al. (2013). Radiative forcing of the direct aerosol effect from AeroCom phase II simulations. *Atmospheric Chemistry and Physics*, *13*(4), 1853–1877. https://doi.org/10.5194/acp-13-1853-2013

Oak Ridge National Laboratory: LandScan Global Population Database (2017). Retrieved from http://web.ornl.gov/sci/landscan/, accessed on August 9.

Ramanathan, V., & Carmichael, G. (2008). Global and regional climate changes due to black carbon. *Nature Geoscience*, *1*(4), 221–227. https://doi.org/10.1038/ngeo156

Samset, B. H., Myhre, G., Schulz, M., Balkanski, Y., Bauer, S., Berntsen, T. K., et al. (2013). Black carbon vertical profiles strongly affect its radiative forcing uncertainty. *Atmospheric Chemistry and Physics*, *13*(5), 2423–2434. https://doi.org/10.5194/acp-13-2423-2013

Sato, M., Hansen, J., Koch, D., Lacis, A., Ruedy, R., Dubovik, O., et al. (2003). Global atmospheric black carbon inferred from AERONET. *Proceedings of the National Academy of Sciences of the United States of America*, *100*(11), 6319–6324. https://doi.org/10.1073/pnas.0731897100

Schulz, M., Textor, C., Kinne, S., Balkanski, Y., Bauer, S., Berntsen, T., et al. (2006). Radiative forcing by aerosols as derived from the AeroCom present-day and pre-industrial simulations. *Atmospheric Chemistry and Physics*, *6*(12), 5225–5246. https://doi.org/10.5194/acp-6-5225-2006

Schutgens, N. A. J., Gryspeerdt, E., Weigum, N., Tsyro, S., Goto, D., Schulz, M., & Stier, P. (2016). Will a perfect model agree with perfect observations? The impact of spatial sampling. *Atmospheric Chemistry and Physics*, *16*(10), 6335–6353. https://doi.org/10.5194/acp-16-6335-2016

Schutgens, N. A. J., Partridge, D. G., & Stier, P. (2016). The importance of temporal collocation for the evaluation of aerosol models with observations. *Atmospheric Chemistry and Physics*, *16*(2), 1065–1079. https://doi.org/10.5194/acp-16-1065-2016

Schutgens, N. J., Tsyro, S., Gryspeerdt, E., Goto, D., Weigum, N., Schulz, M., & Stier, P. (2017). On the spatio-temporal representativeness of observations. *Atmospheric Chemistry and Physics*, *17*(16), 9761–9780. https://doi.org/10.5194/acp-17-9761-2017

Shindell, D. T., Lamarque, J. F., Schulz, M., Flanner, M., Jiao, C., Chin, M., et al. (2013). Radiative forcing in the ACCMIP historical and future climate simulations. *Atmospheric Chemistry and Physics*, *13*(6), 2939–2974. https://doi.org/10.5194/acp-13-2939-2013

Silcox, G. D., Kelly, K. E., Crosman, E. T., Whiteman, C. D., & Allen, B. L. (2012). Wintertime $PM_{2.5}$ concentrations during persistent, multi-day cold-air pools in a mountain valley. *Atmospheric Environment*, *46*, 17–24.

Silva, C., & Quiroz, A. (2003). Optimization of the atmospheric pollution monitoring network at Santiago de Chile. *Atmospheric Environment*, *37*(17), 2337–2345. https://doi.org/10.1016/S1352-2310(03)00152-3

Trujillo-Ventura, A., & Ellis, J. H. (1991). Multiobjective air pollution monitoring network design. *Atmospheric Environment, Part A. General Topics*, *25*(2), 469–479. https://doi.org/10.1016/0960-1686(91)90318-2

Wang, Q. Q., Jacob, D. J., Spackman, J. R., Perring, A. E., Schwarz, J. P., Moteki, N., et al. (2014). Global budget and radiative forcing of black carbon aerosol: Constraints from pole-to-pole (HIPPO) observations across the Pacific. *Journal of Geophysical Research: Atmospheres*, *119*, 195–206. https://doi.org/10.1002/2013JD020824

Wang, R., Balkanski, Y., Boucher, O., Ciais, P., Schuster, G. L., Chevallier, F., et al. (2016). Estimation of global black carbon direct radiative forcing and its uncertainty constrained by observations. *Journal of Geophysical Research: Atmospheres*, *121*, 5948–5971. https://doi.org/10.1002/2015JD024326

Wang, R., Tao, S., Balkanski, Y., Ciais, P., Boucher, O., Liu, J., et al. (2014). Exposure to ambient black carbon derived from a unique inventory and high-resolution model. *Proceedings of the National Academy of Sciences of the United States of America*, *111*(7), 2459–2463. https://doi.org/10.1073/pnas.1318763111

Whiteman, C. D. (2000). *Mountain meteorology: Fundamentals and applications*. New York: Oxford University Press.

WMO (2016). WMO/GAW aerosol measurement procedures, guidelines, and recommendations, WMO TD No. 1177, GAW Report No. 227, World Meteorological Organization, Geneva, Switzerland. Retrieved from https://library.wmo.int/opac/doc_num.php?explnum_id=3073, accessed on August 9, 2017.

Wu, L., Bocquet, M., & Chevallier, M. (2010). Optimal reduction of the ozone monitoring network over France. *Atmospheric Environment*, *44*(25), 3071–3083. https://doi.org/10.1016/j.atmosenv.2010.04.012